INFERENCE-TIME SEARCH USING SIDE INFORMATION FOR DIFFUSION-BASED IMAGE RECONSTRUCTION

Anonymous authors
Paper under double-blind review

ABSTRACT

Diffusion models have emerged as powerful priors for solving inverse problems. However, existing approaches typically overlook side information that could significantly improve reconstruction quality, especially in severely ill-posed settings. In this work, we propose a novel inference-time search algorithm that guides the sampling process using the side information in a manner that balances exploration and exploitation. This enables more accurate and reliable reconstructions, providing an alternative to the gradient-based guidance that is prone to reward-hacking artifacts. Our approach can be seamlessly integrated into a wide range of existing diffusion-based image reconstruction pipelines. Through extensive experiments on a number of inverse problems, such as box inpainting, super-resolution, and various deblurring tasks including motion, Gaussian, nonlinear, and blind deblurring, we show that our approach consistently improves the qualitative and quantitative performance of diffusion-based image reconstruction algorithms. We also show the superior performance of our approach with respect to other baselines, including reward gradient-based guidance algorithms. Code is available here.

1 INTRODUCTION

Diffusion models (Ho et al., 2020; Song et al., 2021b) have demonstrated remarkable success in generative tasks across various fields like text-to-image synthesis (Rombach et al., 2022), protein sequence (Wu et al., 2024), video (Ho et al., 2022), audio (Kong et al., 2021), and language modeling (Austin et al., 2021; Sahoo et al., 2024). Aside from generation, these models have also shown great promise in *solving inverse problems*, where the goal is to reconstruct an image from partial or noisy observations (Chung et al., 2023b; Song et al., 2023a; Rout et al., 2023; Song et al., 2024; He et al., 2024; Ye et al., 2024; Zhang et al., 2024). Inverse problems differ fundamentally from standard generative tasks (e.g., text-to-image synthesis, personalized editing, style transfer): whereas those tasks are often judged subjectively, inverse problems have a precise objective, to recover a specific ground-truth signal from incomplete measurements. Consequently, fidelity to the ground truth and rigorous quantitative evaluation are critical.

When the observation is heavily degraded, the inverse problem becomes highly ill-posed as many distinct signals can explain the data almost equally well. In this regime, unconstrained posterior sampling rarely recovers the ground truth; it tends instead to produce diverse yet semantically inconsistent reconstructions. A practical solution is to incorporate **side information**, auxiliary measurements correlated with the target signal, to constrain the solution space and steer the reconstruction toward faithful outcomes. This idea is well established in the classical signal processing literature, where certain structural or encoded properties are used to guide the iterative algorithms that solve the inverse problem (Jones, 2009; Chun et al., 2012; Oymak et al., 2013; Ehrhardt et al., 2014; Mota et al., 2017; Hyder et al., 2019). In medical imaging, leveraging complementary measurements or modalities, such as multiple MRI contrasts, multimodal microscopy, or RGB guidance for NIR imaging, has been shown to substantially improve quality (Atalık et al., 2025; Tsiligianni & Deligiannis, 2019).

While the existing works on diffusion-based solvers have made significant progress on measurement-only inverse problems, they largely sidestep the harder and increasingly common setting where we must also exploit side information (e.g., a reference photograph of the same person, a text description, or features from another modality). A key obstacle is the challenge of learning the conditional distribution $p_{X|Y,S}$, where X denotes the target image, Y denotes the noisy measurement, and S denotes the side information. While some recent works (Kim et al., 2025a; Chung et al., 2025) address the limited setting of textual side information, these approaches typically train a diffusion

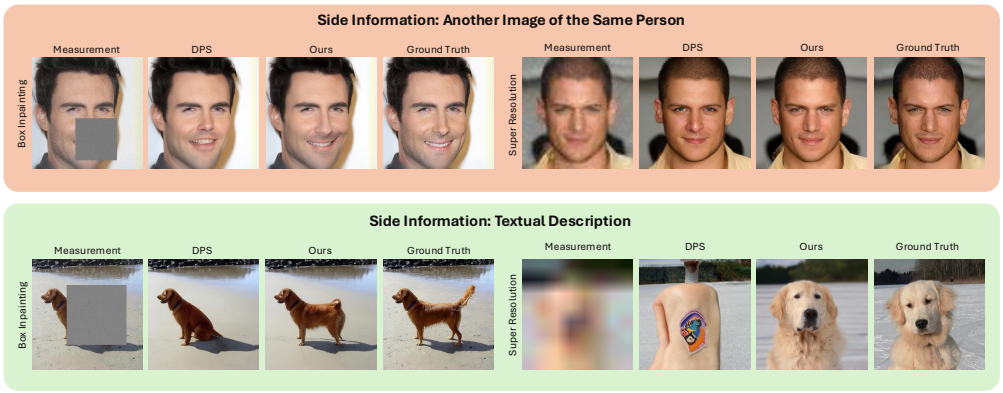

Figure 1: Illustration of the performance of our inference-time search algorithm for using side information in solving inverse problems, compared with the DPS algorithm (Chung et al., 2023b).

model to take a specific side-info modality as input; this demands large paired datasets and expensive training, ties the solver to a single conditioning format, and is impractical when the test-time side information differs from what the model was trained on. This motivates us to address the following question:

How can we leverage a pre-trained (unconditional) diffusion prior to solve inverse problems with side information at inference time, without any retraining, so that the method is modality-agnostic and can use text, images, or features depending on the end-use applications? We provide constructive solutions to these questions in our work. Our main contributions are the following.

- **Modeling:** We introduce a general modeling approach that incorporates arbitrary side information via an auxiliary reward, characterizing $p_{X|S}$ as a reward-tilted version of the pre-trained diffusion prior. This abstraction cleanly decouples the measurement model from the side information, is modality-agnostic (text, image, features), and requires no retraining. We use this modeling with tractable approximations and appropriate error bounds for computing the conditional score functions that are needed for sampling from the pre-trained diffusion models.
- **Algorithm:** Motivated by recent successes of inference-time search in LLMs (Snell et al., 2025; Setlur et al., 2025; Liu et al., 2025), we propose a compute-aware, training-free inference-time search framework that can leverage the side information to solve inverse problems. We instantiate this framework by proposing two specific search algorithms: (i) Greedy Search (GS), a strategy that resamples greedily at each step, and (ii) Recursive Fork-Join Search (RFJS), which balances exploration and exploitation through a group-based sampling at each step. The framework operates as a plug-in on top of any standard inverse-problem solvers and supports black-box, non-differentiable rewards. To our knowledge, our work is the first to propose inference-time search with side information for diffusion-based inverse problems.
- **Experiments:** We provide extensive experimental evaluations of our proposed approach across linear and nonlinear problems (e.g., box inpainting, super-resolution, motion/Gaussian/nonlinear deblurring) and side-information types (images and text), and demonstrate that our approach outperforms multiple relevant baseline algorithms.

2 Related Work

Inverse problems with diffusion priors: Diffusion models (Dhariwal & Nichol, 2021; Ho et al., 2020; Song & Ermon, 2019; Sohl-Dickstein et al., 2015; Song & Ermon, 2020; Song et al., 2021a) are powerful generative models that sample from data distributions by iteratively denoising random noise. Several works adapt diffusion priors to inverse problems via likelihood score approximations. Diffusion Posterior Sampling (DPS) (Chung et al., 2023b) is a foundational method for solving inverse problems in a principled way. Its key idea is to approximate the expected conditional likelihood by evaluating the likelihood at the conditional mean, effectively pushing the expectation through the nonlinear function (Sec. 3.1). ΠGDM (Song et al., 2023a) solves linear inverse problems using a better

approximation than DPS; MPGD (He et al., 2024) avoids this cost by enforcing data consistency in image space; MCG (Chung et al., 2022) constrains reconstructions via manifold projections; DDRM (Kawar et al., 2022) operates in spectral space; and DAPS (Zhang et al., 2024) decouples diffusion steps. Latent diffusion priors are also used: PSLD (Rout et al., 2023) adds consistency terms, ReSample (Song et al., 2024) solves per-step optimization problems, and Chung et al. (2024) tunes prompts for efficiency. None of these methods, however, leverage side information.

Inverse problems with side information: Many works in signal processing (Mota et al., 2017; Oymak et al., 2013; Jones, 2009; Chun et al., 2012; Ehrhardt et al., 2014; Hyder et al., 2019) integrate structural correlations from auxiliary signals, often via designing appropriate optimization algorithms. In MRI, LeSITA (Tsiligianni & Deligiannis, 2019) learns coupled sparse representations, and TGVN (Atalık et al., 2025) constrains ambiguous subspaces with additional contrasts using learned unrolled networks. Diffusion-based approaches include training with joint priors across modalities (Levac et al., 2023; Efimov et al., 2025), metadata conditioning (Chung et al., 2025), and text-guided regularization (Kim et al., 2025a). Most approaches, however, are training-based or bound to one modality of side information associated with the trained conditional diffusion model.

Reward-gradient guidance: LGD (Song et al., 2023b) refines DPS via Monte Carlo estimates, while UGD (Bansal et al., 2024), FreeDoM (Yu et al., 2023), and RB-Modulation (Rout et al., 2025) propose to guide the diffusion with a gradient of the reward function. In addition to being gradient-based approaches, they are typically used for semantic generation tasks rather than inverse problems.

SMC methods: Sequential Monte Carlo approaches (Cardoso et al., 2024; Dou & Song, 2024; Wu et al., 2023) generate and resample particles under tilted distributions, offering gradient-free alternatives but limited performance at small N. DAS (Kim et al., 2025b) combines resampling with gradients for text-to-image tasks. These methods rely only on the measurement to guide the unconditional sampler and do not exploit side information.

Inference-time search: Reward-guided inference-time search has advanced LLM reasoning using Process Advantage Verifiers (PAVs) (Setlur et al., 2025), compute-optimal scheduling (Snell et al., 2025), and reward-guided small models (Liu et al., 2025). Some recent works (Singhal et al., 2025; Li et al., 2025) apply reward-based search in diffusion for text-to-image/protein generation, but do not consider side information or inverse problems.

3 Preliminaries and Problem Formulation

3.1 Preliminaries

Diffusion models: Diffusion models (Ho et al., 2020; Song et al., 2021b) are powerful generative models that enable sampling from an (unknown) distribution through an iterative process. Diffusion models comprise a forward diffusion process and a reverse denoising process. During the forward process, a clean sample from the distribution p_{data} is progressively corrupted by the addition of Gaussian noise at each timestep, transforming the data distribution into pure noise. Conversely, the reverse process trains a denoising neural network to iteratively remove this introduced noise, enabling the reconstruction of samples from the initial data distribution. The forward process is represented by the stochastic differential equation (SDE), $\mathrm{d}\mathbf{x}_t = f(\mathbf{x}_t, t)\mathrm{d}t + g(t)\mathrm{d}\mathbf{w}_t,\ \forall t \in [0, T]$, where x_0 is sampled from p_{data} and $\mathbf{w}_t$ is a Wiener process. Common choices for f, g are $f(\mathbf{x}_t, t) = -(\beta(t)/2)\mathbf{x}_t$ and $g(t) = \sqrt{\beta(t)}$ for some non-negative monotonic increasing function $\beta(\cdot)$ over $[0, T]$. The corresponding reverse process of this SDE is described by (Anderson, 1982; Song et al., 2021b) $\mathrm{d}\mathbf{x}_t = \big(f(\mathbf{x}_t, t) - g^2(t)\nabla_{\mathbf{x}_t} \log p_t(\mathbf{x}_t)\big)\,\mathrm{d}t + \mathrm{d}\mathbf{w}_t,\ \forall t \in [T, 0]$, where p_t denotes the marginal probability distribution of $\mathbf{x}_t$, $\mathbf{x}_T$ is sampled according to a standard Gaussian distribution, and $\nabla_{\mathbf{x}_t} \log p_t(\mathbf{x}_t)$ represents the *score function*. Since the marginal distribution p_t is unknown, the score function is approximated by a neural network $\mathcal{D}_{\boldsymbol{\theta}}(\mathbf{x}_t, t)$ via the minimization of a score-matching objective. In practical implementations, the SDE is discretized into T steps, and we define $\alpha_t \triangleq \prod_{s=1}^{t}(1 - \beta_s)$.

Solving inverse problems using diffusion models: An inverse problem consists of recovering an unknown signal $\mathbf{x}_0$ from noisy, partial observations $\mathbf{y} = \mathbf{A}(\mathbf{x}_0) + \sigma_y \mathbf{z}$, where $\mathbf{A}$ is the measurement model, σ_y is the observation noise level, and $\mathbf{z}$ is typically a Gaussian noise. Often, $\mathbf{A}$ is non-injective, i.e., multiple signals $\mathbf{x}_0$ can produce the same measurement $\mathbf{y}$. A standard approach for estimating $\mathbf{x}_0$ is via the Bayesian framework, assuming a prior distribution p_0 over the signal $\mathbf{x}_0$, and sampling from the posterior distribution $\mathbf{x}_0 \sim p_{0|Y}(\cdot \mid \mathbf{y})$. Though $p_{0|Y}(\cdot \mid \mathbf{y})$ is not

known, this sampling can be achieved by running the backward SDE with replacing the original score function with the conditional score function $\nabla_{\mathbf{x}_t} \log p_{t|Y}(\mathbf{x}_t \mid \mathbf{y})$. Using Bayes' theorem, $\nabla_{\mathbf{x}_t} \log p_{t|Y}(\mathbf{x}_t \mid \mathbf{y}) = \nabla_{\mathbf{x}_t} \log p_t(\mathbf{x}_t) + \nabla_{\mathbf{x}_t} \log p_{Y|t}(\mathbf{y} \mid \mathbf{x}_t)$. While the score function network $\mathcal{D}_{\boldsymbol{\theta}}$ of the pre-trained diffusion model can be used to approximate the first term, approximating the second term is significantly more challenging, and numerous approaches (Daras et al., 2024) have been proposed to tackle this challenge. In particular, Diffusion Posterior Sampling (DPS) (Chung et al., 2023b) proposes a simple approach to approximate $p_{Y|t}$ as $p_{Y|t}(\mathbf{y} \mid \mathbf{x}_t) = \mathbb{E}_{\mathbf{x}_0 \sim p_{0|t}(\cdot|\mathbf{x}_t)}[p_{Y|0}(\mathbf{y} \mid \mathbf{x}_0)] \approx p_{Y|0}(\mathbf{y} \mid \mathbb{E}_{\mathbf{x}_0 \sim p_{0|t}(\cdot|\mathbf{x}_t)}[\mathbf{x}_0])$, by pushing the expectation inside the nonlinear $p_{Y|0}(\mathbf{y} \mid \cdot)$. The remaining challenge is to compute the conditional mean $\mathbb{E}_{\mathbf{x}_0 \sim p_{0|t}(\cdot|\mathbf{x}_t)}[\mathbf{x}_0] \triangleq \hat{\mathbf{x}}_{0|t}(\mathbf{x}_t)$, which is typically tackled by using Tweedie's formula (Efron, 2011), leveraging the fact that $\mathbf{x}_t$ given $\mathbf{x}_0$ is Gaussian. This results in the estimate

$$\hat{\mathbf{x}}_{0|t}(\mathbf{x}_t) = (1/\sqrt{\alpha_t})(\mathbf{x}_t + (1-\alpha_t)\nabla_{\mathbf{x}_t} \log p_t(\mathbf{x}_t)) \approx (1/\sqrt{\alpha_t})(\mathbf{x}_t + (1-\alpha_t)\mathcal{D}_{\boldsymbol{\theta}}(\mathbf{x}_t, t)). \quad (1)$$

3.2 Problem formulation: solving inverse problems with side information

In many applications, the observation $\mathbf{y}$ alone is insufficient to identify the latent signal $\mathbf{x}_0$; auxiliary side information $\mathbf{s}$ (e.g., a reference image, identity/text embedding, or physics-derived features) can dramatically reduce ambiguity. Formally, when side information $\mathbf{s}$ is available, *the goal is to sample from the target conditional distribution* $p_{0|Y,S}(\cdot \mid \mathbf{y}, \mathbf{s})$. A seemingly direct route is to *train a conditional diffusion model* that accepts $\mathbf{s}$ as input, learn the conditional score function $\nabla_{\mathbf{x}_t} \log p_{t|S}(\mathbf{x}_t \mid \mathbf{s})$, and then approximate the full conditional score $\nabla_{\mathbf{x}_t} \log p_{t|Y,S}(\mathbf{x}_t \mid \mathbf{y}, \mathbf{s}) = \nabla_{\mathbf{x}_t} \log p_{t|S}(\mathbf{x}_t \mid \mathbf{s}) + \nabla_{\mathbf{x}_t} \log p_{Y|t,S}(\mathbf{y} \mid \mathbf{x}_t, \mathbf{s})$ through a DPS-style method for the second term, to run the backward SDE. However, this training-based approach is often impractical: it demands large paired datasets $(\mathbf{x}_0, \mathbf{s})$, which are expensive or impossible to curate; it locks the solver to the training modality of $\mathbf{s}$ (a text-conditioned prior cannot natively exploit an image or spectral feature at test time); and general multi-modal conditioning requires prohibitive data and compute. These constraints motivate a training-free alternative that reuses strong unconditional diffusion priors and uses $\mathbf{s}$ only at inference, preserving modality-agnosticism and avoiding costly data collection.

Designing such a training-free method is technically challenging. First, DPS-style derivations rely on tractable likelihoods (e.g., Gaussian $p_{Y|0}$), whereas realistic $p_{S|0}$ are often non-Gaussian implicitly, complicating conditional-score construction. Second, even for measurement-only guidance, computing the conditional score used in the DPS-style algorithms requires back-propagating through the denoiser at every step. Naively extending to side information forces second-order/Hessian terms through the diffusion network. Third, purely gradient-guided diffusion is brittle: it struggles with non-differentiable or black-box rewards, amplifies early-step errors, and can drift off the data manifold. Inference-time search approaches, which have shown remarkable performance improvement in LLMs (Setlur et al., 2025; Liu et al., 2025; Snell et al., 2025) and text-conditioned diffusion models (Singhal et al., 2025; Kim et al., 2025b), but have not yet been used for solving the inverse problems, offer a promising path to overcome these challenges. In this context, we address the following questions:

(i) *Modeling:* How can we realize $p_{0|Y,S}$ at inference time, without any retraining, by constructing a surrogate objective that is valid across diverse side-information modalities? (ii) *Algorithm*: How can we design a plug-and-play inference-time search module that is modality-agnostic, compute-aware, and capable of making global corrections (beyond local gradient steps)?

4 Modeling and Algorithm

4.1 Modeling side information using reward function

Given a side-information signal $\mathbf{s}$ corresponding to an unknown $\mathbf{x}_0$, and two candiate reconstructions, $\mathbf{x}_0^1$ and $\mathbf{x}_0^2$, a principled way to decide which reconstruction is more truthful is to compare the (unknown) conditional probabilities $p_{0|S}(\mathbf{x}_0^1 \mid \mathbf{s})$ and $p_{0|S}(\mathbf{x}_0^2 \mid \mathbf{s})$. Directly estimating $p_{0|S}$ is intractable in our setting: it is typically non-Gaussian, multi-modal, and depends on the data domain and modality of $\mathbf{s}$. We therefore introduce a reward function $r : \mathbb{R}^d \times \mathcal{S} \to \mathbb{R}$ that orders reconstructions given $\mathbf{s}$: if $r(\mathbf{x}_0^1, \mathbf{s}) > r(\mathbf{x}_0^2, \mathbf{s})$, then $\mathbf{x}_0^1$ is deemed more compatible with $\mathbf{x}_0$ than $\mathbf{x}_0^2$. This abstraction aligns with many real-world applications (as shown in our experiments): when $\mathbf{s}$ is a text description of the target image $\mathbf{x}_0$, we can use a pre-trained text-image model to score text-image alignment. When $\mathbf{s}$ is a reference image of the same entity (e.g., the same person under different poses/lighting), we can use a pre-trained network to score image-image similarity. Such pre-trained

rewards are typically available across datasets, and monotone with respect to the intuitive notion of *agreement* with $\mathbf{x}_0$. In this sense, they serve as practically justified surrogates for comparing $p_{0|S}$ without requiring an explicit conditional density model.

Our key modeling choice is to use $r(\cdot, \mathbf{s})$ to implicitly characterize $p_{0|S}(\cdot \mid \mathbf{s})$ by tilting the unconditional prior p_0 toward higher-reward regions. Our approach is inspired by the alignment framework used in LLMs (Ouyang et al., 2022; Rafailov et al., 2023), where the goal is to generate a sample $\mathbf{x}$ that maximizes some reward $r(\mathbf{x})$, while ensuring that the sampling distribution does not deviate too much from the pre-trained distribution p_0. This is typically formalized as a KL-regularized reward maximization problem, $\max_{p \in \mathcal{P}} \left(\mathbb{E}_{\mathbf{x} \sim p}[r(\mathbf{x})] - \tau D_{\mathrm{KL}}(p \| p_0) \right)$, where $\tau > 0$ offers the trade-off between the deviation from the prior and reward maximization. This optimization problem admits a closed-form solution, $p^*(\mathbf{x}) \propto p_0(\mathbf{x}) \exp(r(\mathbf{x})/\tau)$ (Rafailov et al., 2023). Based on this intuition, we make the following *modeling assumption*: the conditional distribution $p_{0|S}$ is approximated as,

$$p_{0|S}(\mathbf{x}_0 \mid \mathbf{s}) \propto p_0(\mathbf{x}_0) \exp\left(\tfrac{r(\mathbf{x}_0; \mathbf{s})}{\tau} \right), \tag{2}$$

This assumption: (i) preserves the powerful unconditional diffusion prior p_0, (ii) injects modality-agnostic side information via a reward, and (iii) produces a tractable objective that we can combine with the measurement model to target $p_{0|Y,S}$ at inference time using a pre-trained diffusion model. We do not claim optimality of Eq. (2); rather, we show it leads to a practical, training-free algorithm that consistently improves reconstructions over strong baselines while keeping compute comparable.

We now leverage Eq. (2) to compute the conditional posteriors for the reverse diffusion.

Proposition 1. *Let $p_{t|t+1,Y,S}$ denote the conditional posterior distribution for the reverse diffusion process. Then using (2) we have*

$$p_{t|t+1,Y,S}(\mathbf{x}_t \mid \mathbf{x}_{t+1}, \mathbf{y}, \mathbf{s}) \propto p_{t|t+1,Y}(\mathbf{x}_t \mid \mathbf{x}_{t+1}, \mathbf{y}) \exp(V_t^\tau(\mathbf{x}_t; \mathbf{s}, \mathbf{y})), \tag{3}$$

$$p_{t|Y,S}(\mathbf{x}_t \mid \mathbf{y}, \mathbf{s}) \propto p_{t|Y}(\mathbf{x}_t \mid \mathbf{y}) \exp(V_t^\tau(\mathbf{x}_t; \mathbf{s}, \mathbf{y})), \tag{4}$$

where $V_t^\tau(\mathbf{x}_t; \mathbf{s}, \mathbf{y}) \triangleq \log \mathbb{E}_{\mathbf{x}_0 \sim p_{0|t,Y}(\cdot|\mathbf{x}_t, \mathbf{y})}[\exp(r(\mathbf{x}_0; \mathbf{s})/\tau)]$.

The proof is provided in Appendix A.1. Using (4), we can get the conditional score function as,

$$\nabla_{\mathbf{x}_t} \log p_{t|Y,S}(\mathbf{x}_t \mid \mathbf{y}, \mathbf{s}) = \nabla_{\mathbf{x}_t} \log p_t(\mathbf{x}_t) + \nabla_{\mathbf{x}_t} \log p_{Y|t}(\mathbf{y} \mid \mathbf{x}_t) + \nabla_{\mathbf{x}_t} V_t^\tau(\mathbf{x}_t; \mathbf{s}, \mathbf{y}). \tag{5}$$

The computation of V_t^τ is not straightforward. So, we use a DPS-style approximation as $V_t^\tau(\mathbf{x}_t; \mathbf{s}, \mathbf{y}) = \log \mathbb{E}_{\mathbf{x}_0 \sim p_{0|t,Y}(\cdot|\mathbf{x}_t, \mathbf{y})}[\exp(r(\mathbf{x}_0; \mathbf{s})/\tau)] \approx r(\mathbb{E}_{\mathbf{x}_0 \sim p_{0|t,Y}(\cdot|\mathbf{x}_t, \mathbf{y})}[\mathbf{x}_0]; \mathbf{s})/\tau = r(\hat{\mathbf{x}}_{0|t,Y}(\mathbf{x}_t, \mathbf{y}); \mathbf{s})/\tau$. Using some approximation and the fact that $p_{Y|0}$ is Gaussian, we can get

$$\hat{\mathbf{x}}_{0|t,Y}(\mathbf{x}_t, \mathbf{y}) \approx \hat{\mathbf{x}}_{0|t}(\mathbf{x}_t) - (1 - \alpha_t)(\sqrt{\alpha_t}))\eta \nabla_{\mathbf{x}_t} \|\mathbf{y} - \mathbf{A}\hat{\mathbf{x}}_{0|t}(\mathbf{x}_t)\|_2^2, \tag{6}$$

$$V_t^\tau(\mathbf{x}_t; \mathbf{s}, \mathbf{y}) \approx \hat{V}_t^\tau(\mathbf{x}_t; \mathbf{s}, \mathbf{y}) \triangleq r\left(\hat{\mathbf{x}}_{0|t,Y}(\mathbf{x}_t, \mathbf{y}); \mathbf{s}\right)/\tau. \tag{7}$$

In Appendix A.2, we have provided the details of the steps leading to Eq. (6)-Eq. (7).

We characterize the error in approximating the value function, $|V_t^\tau(\mathbf{x}_t; \mathbf{s}, \mathbf{y}) - \hat{V}_t^\tau(\mathbf{x}_t; \mathbf{s}, \mathbf{y})|$, in Proposition 3, which is deferred to Appendix A.2.

We can now get $\nabla_{\mathbf{x}_t} \log p_{t|Y,S}(\mathbf{x}_t \mid \mathbf{y}, \mathbf{s})$ given in Eq. (5) by replacing $\nabla_{\mathbf{x}_t} V_t^\tau(\mathbf{x}_t; \mathbf{s}, \mathbf{y})$ with $\nabla_{\mathbf{x}_t} \hat{V}_t^\tau(\mathbf{x}_t; \mathbf{y}, \mathbf{s})$. However, running a backward diffusion using $\nabla_{\mathbf{x}_t} \hat{V}_t^\tau(\mathbf{x}_t; \mathbf{s}, \mathbf{y})$ is computationally infeasible because it involves computing second-order derivatives through the denoiser network. This issue, however, can be circumvented by making a further approximation, by setting $\eta = 0$ in Eq. (6) to get $\hat{\mathbf{x}}_{0|t,Y}(\mathbf{x}_t, \mathbf{y}) \approx \hat{\mathbf{x}}_{0|t}(\mathbf{x}_t)$, which leads to the approximation $\nabla_{\mathbf{x}_t} V_t^\tau(\mathbf{x}_t; \mathbf{s}, \mathbf{y}) \approx \nabla_{\mathbf{x}_t} r(\hat{\mathbf{x}}_{0|t}(\mathbf{x}_t); \mathbf{s})$. We show that approximation error remains small when t is small in Appendix A.2 even when $\eta = 0$. This approach then reduces to the **reward gradient guidance (RGG)** approach used for the inference-time alignment of diffusion models (Bansal et al., 2024; Kim et al., 2025b; Yu et al., 2023; He et al., 2024), with the critical difference being that the guidance is from both $\mathbf{s}$ and $\mathbf{y}$.

The RGG approach, however, is limited only to differentiable rewards, and even when they are differentiable, calculating a gradient through the denoiser network at each step of the backward diffusion is computationally intensive and can be ill-suited for many end-use edge-device applications. Moreover, the hyperparameter that determines the weight of the reward gradient guidance is highly sensitive and is difficult to tune, leading to limited performance improvements and undesirable artifacts in the reconstructed images. We later illustrate these issues in Appendix B.6. This motivates us to pursue a gradient-free approach for leveraging the side information for inverse problems.

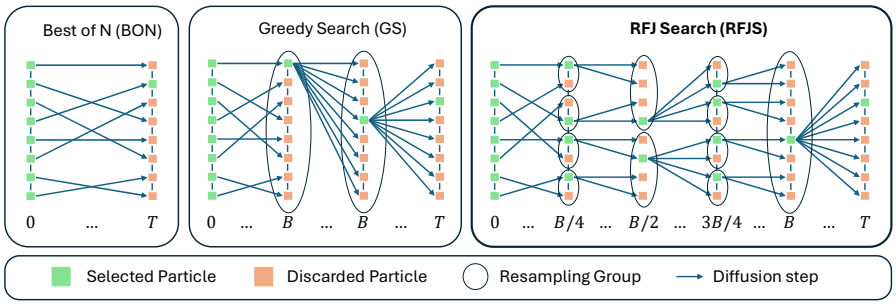

Figure 2: Illustration of the group size resampling strategies of different search algorithms.

4.2 Inference-time Search Algorithms for Inverse Problems

Inference-time search methods have recently gained traction as a means of improving the quality of output from LLMs (Snell et al., 2025; Setlur et al., 2025; Liu et al., 2025). The key objective of a search algorithm is to solve a multi-step decision-making problem with balanced exploration and exploitation. While Monte Carlo Tree Search (MCTS) (Kocsis & Szepesvári, 2006) was successful in large-scale reinforcement learning systems like AlphaGo (Silver et al., 2016), they are infeasible for diffusion models: estimating the expected reward of a noisy state $\mathbf{x}_t$ would require repeated rollouts of the reverse process. Training a value function to guide the search rewards is another alternative, but this demands additional training customized to each modality and type of side information. These limitations motivate inference-time methods that are both training-free and computationally tractable.

Particle-based procedures offer one such approach, using the distribution given by Eq. (3), where the value function is replaced by the approximation in Eq. (7). At a given step, suppose we have N samples $\mathbf{x}_{t+1}[1], \ldots, \mathbf{x}_{t+1}[N] \sim p_{t+1|Y,S}$. One way to generate samples from $p_{t|Y,S}$ is to (i) propose candidates $\tilde{\mathbf{x}}_t[i] \sim p_{t|t+1,Y}(\cdot \mid \mathbf{x}_{t+1}[i], \mathbf{y})$, (ii) compute rewards $r[i] = r(\hat{\mathbf{x}}_{0|t,Y}(\tilde{\mathbf{x}}_t[i], \mathbf{y}); \mathbf{s})$ (approximate value) (iii) assign weights $w[i] \propto \exp(r[i]/\tau)$ and resample indices with replacement $I[i] \sim \mathrm{Cat}(w[1:N])$, and (iv) retain $\mathbf{x}_t[I[i]]$ for the next step. In theory, such particle methods converge to the target distribution as $N \to \infty$ and with exact tilting (Wu et al., 2023; Dou & Song, 2024). In practice, however, finite N and approximate tilting has some issues: frequent resampling favors exploitation but risks reward over-optimization, while no resampling preserves data consistency but requires prohibitively many particles to harness and optimize the reward.

To address this trade-off, we modify the step (iii) by introducing **grouped resampling** at each time step t, where particles are resampled within groups of size g_t. Formally, let the index set of the i-th group be $\mathcal{G}_i = \{(i-1)g_t + 1, \ldots, ig_t\}$ for $i = 1, \ldots, N/g_t$. For each group, we draw g_t indices with replacement according to the weights within that groups, i.e., $I'[j] \sim \mathrm{Cat}(w[\mathcal{G}_i]) \in [1 : g_t]$. The absolute indices are then obtained by shifting I' as $I[(i-1)g_t + j : ig_t + j] = (i-1)g_t + I'[j]$ for $j = 1, \ldots, g_t$. Based on the choice of g_t, we introduce two specific search strategies.

Greedy Search (GS): Here, we use a fixed resampling period B and select $g_t = N$ whenever $t \bmod B = 0$, and $g_t = 1$ otherwise. Greedy Search reduces to the **Best-of-N** (BON) strategy when $B \geq T$, since in that case $g_t = 1$ for all t. Smaller values of B emphasize short-term reward exploitation, while larger values promote long-term consistency and exploration. An illustration of Greedy Search, with resampling interval B, is provided in Figure 2, where the particles evolve independently between resampling events and only interact at steps that are multiples of B.

Recursive Fork-Join Search (RFJS): Greedy search considers the largest resampling group size (N) at fixed time periods of B, and greedily selects one particle from this group, which leads to an exploitation-style approach in search. Selecting the smallest group size $(g_t = 1)$ leads to a pure exploration-style search of BON. Ideally, one should combine the benefits of resampling with multiple group sizes at multiple time steps to get a balanced exploration and exploitation.

To this end, we propose a *recursive grouping and sampling approach*, which we call recursive fork-join search (RFJS), in which the resampling group sizes vary systematically over time. At every B steps, all N particles are resampled together; at every $B/2$ steps, the particles are partitioned into groups of size $N/2$ that are resampled independently; at every $B/4$ steps, groups of size $N/4$ are resampled; and so on. This hierarchical schedule is illustrated in Figure 2. As a concrete example,

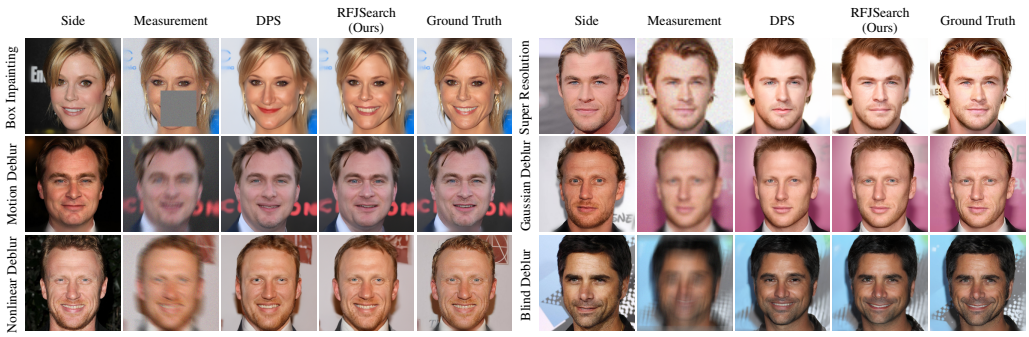

Figure 3: **Image as side information:** Qualitative illustration of the performance of our RFJS algorithm compared to the DPS baseline on linear and nonlinear inverse problems. RFJS is able to capture many details that are missed by the DPS baseline to achieve a superior reconstruction quality.

	Box Inpainting				Super Resolution (×4)				Non-linear Deblur			
Algorithm	FS (↓)	PSNR (↑)	LPIPS (↓)	SSIM (↑)	FS (↓)	PSNR (↑)	LPIPS (↓)	SSIM (↑)	FS (↓)	PSNR (↑)	LPIPS (↓)	SSIM (↑)
RFJS (ours)	**0.308**	**28.29**	**0.136**	**0.855**	**0.380**	**25.26**	**0.225**	0.695	**0.394**	23.89	**0.229**	0.668
GS (ours)	0.349	28.22	0.137	0.855	0.460	25.24	0.225	**0.696**	0.467	**23.92**	0.232	**0.669**
RGG	0.475	27.96	0.138	0.851	0.573	25.13	0.228	0.690	0.654	23.89	0.231	0.665
BON	0.584	28.20	0.137	0.854	0.915	25.14	0.229	0.694	0.881	23.89	0.233	0.667
DPS	0.739	27.93	0.139	0.852	1.042	25.13	0.229	0.693	1.008	23.87	0.232	0.666
	Motion Deblur				Gaussian Deblur				Blind Deblur			
RFJS (ours)	**0.326**	**26.64**	**0.193**	**0.736**	**0.330**	**26.20**	**0.196**	**0.712**	**0.341**	25.04	**0.209**	0.707
GS (ours)	0.392	26.58	0.193	0.735	0.385	26.16	0.198	0.711	0.417	25.04	0.211	0.706
RGG	0.497	26.55	0.193	0.733	0.495	26.15	0.200	0.709	0.473	24.97	0.211	0.701
BON	0.671	26.57	0.194	0.735	0.667	26.18	0.201	0.711	0.642	**25.15**	0.210	**0.708**
DPS	0.815	26.54	0.194	0.734	0.807	26.15	0.200	0.711	0.779	24.98	0.213	0.704

Table 1: **Image as side information:** Quantitative comparison of our GS and RFJS algorithms with baseline algorithms. For each evaluation metric, the best result is shown in **bold**, and the second best is underlined. RFJS and GS achieve superior performance consistently across all tasks and metrics.

consider $N = 8$. In this case, groups of size at least $N/4 = 2$ are resampled every $B/4$ steps, groups of size $N/2 = 4$ are resampled every $B/2$ steps, and all $N = 8$ particles are resampled every B steps. When multiple group sizes are scheduled to be resampled at the same time step t, the larger group size always takes precedence. For example, although $t = B/2$ is also a multiple of $B/4$, the scheme prioritizes the larger group size. Thus, rather than resampling groups of size 2, we resample groups of size 4 at $t = B/2$. Similarly, at $t = B$, the entire set of $N = 8$ particles is resampled jointly. More generally, the group size at time step t is given by $g_t = N/2^{j^*}$, where $j^* = \min\{\, i \geq 0 : \; t \bmod (B/2^i) = 0 \,\}$. The localized resampling (fork) at intermediate group sizes encourages balanced exploration, while the recursive return to larger group sizes (join) encourages exploitation. Naively reducing B in GS does not balance this trade-off well and may lead to an undesirable compromise between exploration and exploitation.

We have summarized this inference-time search framework in Algorithm 1 in the Appendix A.3. Our framework is modular: the resampling rule, whether BON, GS, or RFJS, can be chosen depending on budget and application. Since this requires no retraining and works with arbitrary reward functions, it can be incorporated into any diffusion-based inverse problem solvers with minimal modification.

5 Experiments

5.1 Experimental Setup

We evaluate our inference-time search framework for solving inverse problems with side information by instantiating two specific search algorithms we proposed: **Greedy Search (GS)** and **Recursive Fork Join Search (RFJS)**, both of which are described in the previous section. We consider two types of side information: (i) **image as side information**, where a reference image of the same entity (here, the same person under different poses/lighting) is used as side information, and (ii) **text as side information**, where a text description of the target image is used as a side information.

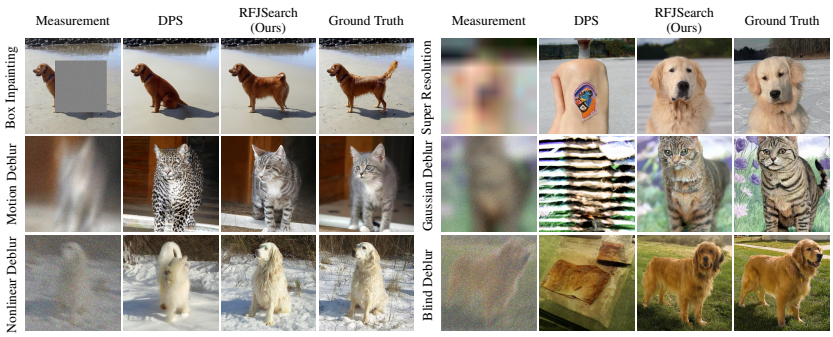

Figure 4: **Text as side information :** Qualitative illustration of the performance of our RFJS algorithm compared to the DPS baseline. For example, the side information provided for the super resolution task is *'golden retriever sitting on a snowy frozen lake, facing forward'*. RFJS is able to capture many details that are missed by the DPS baseline to achieve a superior reconstruction quality.

	Box Inpainting				Super Resolution (×32)				Non-linear Deblur			
Algorithm	CS (↑)	PSNR (↑)	SSIM (↑)	LPIPS (↓)	CS (↑)	PSNR (↑)	SSIM (↑)	LPIPS (↓)	CS (↑)	PSNR (↑)	SSIM (↑)	LPIPS (↓)
RFJS (ours)	**0.901**	**20.75**	**0.678**	**0.294**	**0.801**	17.13	**0.352**	**0.4926**	0.863	**20.58**	**0.473**	**0.405**
GS (ours)	0.894	19.76	0.676	0.305	0.791	17.20	0.351	0.5094	**0.865**	20.32	0.456	0.405
BON	0.882	19.99	0.672	0.308	0.788	**17.21**	0.350	0.5003	0.855	20.52	0.464	0.406
DPS	0.871	19.86	0.672	0.312	0.731	16.90	0.330	0.5220	0.839	20.55	0.469	0.409
	Motion Deblur				Gaussian Deblur				Blind Deblur			
RFJS (ours)	**0.858**	18.61	0.402	**0.424**	**0.843**	**18.10**	0.358	0.457	**0.851**	18.84	0.412	**0.433**
GS (ours)	0.835	17.83	0.369	0.453	0.835	17.96	0.356	0.457	0.835	**18.93**	**0.414**	0.438
BON	0.848	**19.24**	**0.415**	0.427	0.831	17.99	**0.365**	**0.452**	0.831	18.78	0.410	0.443
DPS	0.794	18.16	0.384	0.458	0.778	16.79	0.329	0.487	0.793	18.82	0.409	0.459

Table 2: **Text as side information:** Quantitative comparison of our GS and RFJS algorithms with baseline algorithms. RFJS and GS achieve better performance across all tasks and metrics.

We demonstrate the plug-and-play nature of our algorithms by considering four different baseline inverse problem solvers: (i) **DPS** (Chung et al., 2023b), (ii) **BlindDPS** (Chung et al., 2023a), (iii) **MPGD** (He et al., 2024), and (iv) **DAPS** (Zhang et al., 2024). Due to page limitation, the evaluation results using DAPS and MPGD are deferred to Appendix B.

Inverse problems: We evaluate our algorithms on six inverse problems, covering both linear and nonlinear problems. The linear problems are: (i) box inpainting, (ii) super resolution, (iii) motion deblurring, and (iv) Gaussian deblurring. The nonlinear problems are: (v) nonlinear deblurring, and (vi) blind deblurring. A detailed description of these inverse problems is given in Appendix C.

Baselines: We compare the performance of GS and RFJS against the following baselines: (i) *Baseline solvers (DPS, BlindDPS, MPGD, DAPS)*, (ii) *Best-of-N (BoN)*, which generates N independent samples and selects the one with the best reward at the end, (iii) *Reward Gradient Guidance (RGG)*, which solves the inverse problem by running the backward diffusion according to Eq. (5), but with the approximation $\nabla_{\mathbf{x}_t} V_t^\tau(\mathbf{x}_t; \mathbf{s}, \mathbf{y}) \approx \nabla_{\mathbf{x}_t} r(\hat{\mathbf{x}}_{0|t}(\mathbf{x}_t); \mathbf{s})$. Unless otherwise noted, hyperparameters, including guidance scale, number of diffusion steps, and task-specific settings, match the original baseline implementations. The specific values of hyperparamaters are listed in Appendix C. All the experiments are run on NVIDIA A100 GPUs on an internal compute cluster.

5.2 Main Results

Image as side information: The goal is to reconstruct a human face from a noisy observation when another image of the same identity is available (Fig. 3). Using Celeb-HQ (Na et al., 2022) as an out-of-distribution set and a diffusion model pretrained on FFHQ (Chung et al., 2023b), we sample two random images per identity for target and side information. We compute the reward as follows: first, detect the face using MTCNN (Zhang et al., 2016) and then extract identity features with AdaFace (Kim et al., 2022). Then, we measure the reward as the negative of the FaceSimilarity (FS) loss, computed as the distance between the identity embeddings of the reconstructed and side-information faces, extracted by pretrained AdaFace network. We evaluate on 64 pairs, using $N = 8$ particles and $B = 16$, with a gradient scale 0.5 for RGG. We evaluate with standard metrics, PSNR, SSIM, and LPIPS, but these often fail to measure the identity similarity. Thus, we use FaceSimilarity (FS),

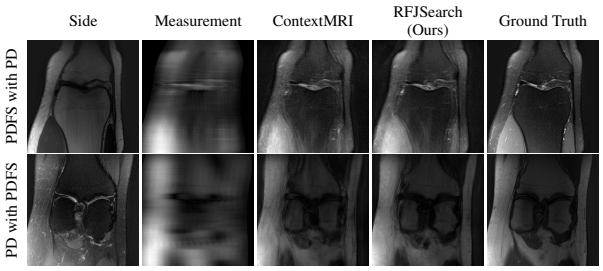

Figure 5: **Contrast Image as Side Information:** Qualitative MRI reconstruction with RFJS vs. ContextMRI. The shapes and line edges are well preserved in our reconstruction.

Algorithm	PSNR (↑)	SSIM (↑)	LPIPS (↓)	NMI (↑)
PDFS with PD				
RFJS	**25.85**	**0.801**	**0.375**	**0.457**
GS	25.33	0.797	0.375	0.455
BON	25.47	0.797	0.376	0.454
ContextMRI	25.39	0.795	0.383	0.451
PD with PDFS				
RFJS	**27.85**	**0.920**	**0.358**	**0.579**
GS	27.80	0.920	0.360	0.579
BON	27.80	0.918	0.366	0.570
ContextMRI	27.46	0.915	0.375	0.563

Figure 6: Quantitative MRI reconstruction results (fastMRI knee, AF=16, ACS=2%).

comparing the reconstruction to the ground truth for a more reliable measure of identity preservation. Table 1 shows that both proposed inference-time search methods, GS and RFJS, outperform baselines, with RFJS achieving the best overall scores indicating a stronger balance between exploration and exploitation. Qualitative results given in Fig 3 show sharper facial details and preserved identity traits, whereas Fig 7 and a detailed discussion in Appendix B.1 indicates the importance of the FS metric.

Text as side information: The goal is to reconstruct an image from its noisy observation, with a text description of the image available as side information. We use a pre-trained diffusion model trained on the ImageNet data (Dhariwal & Nichol, 2021). We use 25 images from the ImageNet validation set to evaluate the algorithms and generated a short one-sentence textual description for each image using ChatGPT. We use ImageReward (Xu et al., 2023), a pre-trained network that measures text-to-image similarity, as the reward function. We consider some inverse problem tasks that are significantly challenging, including $\times 32$ super resolution, and strong blur with larger kernels. Experiments use $N{=}4$ and $B{=}100$, and we report the standard metrics and CLIPScore (Radford et al., 2021). CLIPScore measures the cosine similarity between CLIP image embeddings of the ground truth and reconstruction, providing a semantically informed metric that reflects both visual and textual alignment. It can be seen in Fig. 4 that the qualitative reconstructions closely match textual descriptions. The quantitative metrics are in Table 2 where both GS and RFJS outperform competing baselines, with RFJS achieving the highest CLIPScore.

MRI with multi-contrast side information: Finally, we test on fastMRI knee dataset (Zbontar et al., 2018) with the ContextMRI model (Chung et al., 2025). We pair PD and PDFS contrasts, reconstructing one from the other under highly accelerated $16\times$ undersampling with 2% ACS. We use normalized mutual information (NMI) as reward, which is robust to contrast changes. Table 6 shows our methods consistently outperform the baseline in all the metrics of interest. Figure 5 highlights sharper edges and more faithful structure.

Additional Experiments: To demonstrate the generality of our framework, we extended our search algorithm beyond DPS to other samplers, including DAPS and MPGD. Qualitative and quantitative results for these experiments are provided in Appendix B, along with additional DPS results for both types of side information. We also conducted several ablations to analyze the role of side information and the scalability of our approach. Appendix B.6 studies the sensitivity of the gradient-guided methods. Appendix B.7 examines the effect of the number of particles: increasing N improves exploration and reward, while runtime grows sublinearly due to parallelization (Appendix B.8). To build intuition, Appendix B.9 provides 2D toy examples illustrating the benefits of side information and the impact of B; Fig. 25 further shows that RFJS is more robust than GS when the reward is non-linear and non-convex. Hyperparameter details are summarized in Appendix C.

6 Conclusion

We proposed a lightweight, modular inference-time search algorithm that integrates side information into diffusion-based image reconstruction, in a principled way. By adaptively guiding the generative process, our method delivers substantial quality gains, especially in ill-posed settings, while requiring only minimal changes to existing pipelines. Extensive experiments across standard reconstruction tasks show consistent improvements in both visual fidelity and quantitative metrics, and our approach surpasses gradient-based alternatives. These results highlight the power of leveraging side information at inference time to make diffusion-based solvers more reliable and accurate.

REFERENCES

Brian D.O. Anderson. Reverse-time diffusion equation models. *Stochastic Processes and their Applications*, 12(3):313–326, 1982. ISSN 0304-4149. doi: https://doi.org/10.1016/0304-4149(82)90051-5. URL https://www.sciencedirect.com/science/article/pii/0304414982900515.

Arda Atalık, Sumit Chopra, and Daniel Sodickson. A Trust-Guided Approach to MR Image Reconstruction with Side Information. *IEEE Transactions on Medical Imaging*, 2025.

Jacob Austin, Daniel D. Johnson, Jonathan Ho, Daniel Tarlow, and Rianne van den Berg. Structured denoising diffusion models in discrete state-spaces. In *Advances in Neural Information Processing Systems*, 2021.

Arpit Bansal, Hong-Min Chu, Avi Schwarzschild, Roni Sengupta, Micah Goldblum, Jonas Geiping, and Tom Goldstein. Universal Guidance for Diffusion Models. In *The Twelfth International Conference on Learning Representations*, 2024.

Gabriel Cardoso, Yazid Janati el idrissi, Sylvain Le Corff, and Eric Moulines. Monte Carlo guided Denoising Diffusion models for Bayesian linear inverse problems. In *The Twelfth International Conference on Learning Representations*, 2024.

Se Young Chun, Jeffrey A. Fessler, and Yuni K. Dewaraja. Non-local means methods using ct side information for i-131 spect image reconstruction. In *2012 IEEE Nuclear Science Symposium and Medical Imaging Conference Record (NSS/MIC)*, 2012.

Hyungjin Chung, Byeongsu Sim, Dohoon Ryu, and Jong Chul Ye. Improving Diffusion Models for Inverse Problems using Manifold Constraints. In *Advances in Neural Information Processing Systems*, 2022.

Hyungjin Chung, Jeongsol Kim, Sehui Kim, and Jong Chul Ye. Parallel Diffusion Models of Operator and Image for Blind Inverse Problems . In *2023 IEEE/CVF Conference on Computer Vision and Pattern Recognition (CVPR)*, 2023a.

Hyungjin Chung, Jeongsol Kim, Michael Thompson Mccann, Marc Louis Klasky, and Jong Chul Ye. Diffusion posterior sampling for general noisy inverse problems. In *The Eleventh International Conference on Learning Representations*, 2023b.

Hyungjin Chung, Jong Chul Ye, Peyman Milanfar, and Mauricio Delbracio. Prompt-tuning latent diffusion models for inverse problems. In *Proceedings of the 41st International Conference on Machine Learning*, 2024.

Hyungjin Chung, Dohun Lee, Zihui Wu, Byung-Hoon Kim, Katherine L Bouman, and Jong Chul Ye. Contextmri: Enhancing compressed sensing mri through metadata conditioning. *arXiv preprint arXiv:2501.04284*, 2025.

Giannis Daras, Hyungjin Chung, Chieh-Hsin Lai, Yuki Mitsufuji, Jong Chul Ye, Peyman Milanfar, Alexandros G Dimakis, and Mauricio Delbracio. A survey on diffusion models for inverse problems. *arXiv preprint arXiv:2410.00083*, 2024.

Prafulla Dhariwal and Alexander Nichol. Diffusion models beat gans on image synthesis. In *Advances in Neural Information Processing Systems*, 2021.

Zehao Dou and Yang Song. Diffusion posterior sampling for linear inverse problem solving: A filtering perspective. In *The Twelfth International Conference on Learning Representations*, 2024.

Timofey Efimov, Harry Dong, Megna Shah, Jeff Simmons, Sean Donegan, and Yuejie Chi. Leveraging multimodal diffusion models to accelerate imaging with side information. In *IEEE International Conference on Acoustics, Speech and Signal Processing (ICASSP)*, 2025.

Bradley Efron. Tweedie's formula and selection bias. *Journal of the American Statistical Association*, 106(496):1602–1614, 2011.

Matthias J Ehrhardt, Kris Thielemans, Luis Pizarro, David Atkinson, Sébastien Ourselin, Brian F Hutton, and Simon R Arridge. Joint reconstruction of pet-mri by exploiting structural similarity. *Inverse Problems*, 2014.

Ian J. Goodfellow, Jonathon Shlens, and Christian Szegedy. Explaining and harnessing adversarial examples. In *International Conference on Learning Representations*, 2015.

Yutong He, Naoki Murata, Chieh-Hsin Lai, Yuhta Takida, Toshimitsu Uesaka, Dongjun Kim, Wei-Hsiang Liao, Yuki Mitsufuji, J Zico Kolter, Ruslan Salakhutdinov, and Stefano Ermon. Manifold preserving guided diffusion. In *The Twelfth International Conference on Learning Representations*, 2024.

Jonathan Ho, Ajay Jain, and Pieter Abbeel. Denoising diffusion probabilistic models. In *Advances in Neural Information Processing Systems*, 2020.

Jonathan Ho, William Chan, Chitwan Saharia, Jay Whang, Ruiqi Gao, Alexey Gritsenko, Diederik P. Kingma, Ben Poole, Mohammad Norouzi, David J. Fleet, and Tim Salimans. Imagen video: High definition video generation with diffusion models. *arXiv preprint arXiv:2210.02303*, 2022.

Rakib Hyder, Chinmay Hegde, and M. Salman Asif. Fourier phase retrieval with side information using generative prior. In *2019 53rd Asilomar Conference on Signals, Systems, and Computers*, 2019.

Lee K. Jones. Local minimax learning of functions with best finite sample estimation error bounds: Applications to ridge and lasso regression, boosting, tree learning, kernel machines, and inverse problems. *IEEE Transactions on Information Theory*, 2009.

Bahjat Kawar, Michael Elad, Stefano Ermon, and Jiaming Song. Denoising diffusion restoration models. In *Advances in Neural Information Processing Systems*, 2022.

Jeongsol Kim, Geon Yeong Park, Hyungjin Chung, and Jong Chul Ye. Regularization by texts for latent diffusion inverse solvers. In *International Conference on Learning Representations*, 2025a.

Minchul Kim, Anil K Jain, and Xiaoming Liu. Adaface: Quality adaptive margin for face recognition. In *Proceedings of the IEEE/CVF Conference on Computer Vision and Pattern Recognition*, 2022.

Sunwoo Kim, Minkyu Kim, and Dongmin Park. Test-time Alignment of Diffusion Models without Reward Over-optimization. In *The Thirteenth International Conference on Learning Representations*, 2025b.

Levente Kocsis and Csaba Szepesvári. Bandit based monte-carlo planning. In *Proceedings of the 17th European Conference on Machine Learning*, 2006.

Zhifeng Kong, Wei Ping, Jiaji Huang, Kexin Zhao, and Bryan Catanzaro. Diffwave: A versatile diffusion model for audio synthesis. In *International Conference on Learning Representations*, 2021.

Brett Levac, Ajil Jalal, Kannan Ramchandran, and Jonathan I. Tamir. MRI Reconstruction with Side Information using Diffusion Models. *2023 57th Asilomar Conference on Signals, Systems, and Computers*, 2023.

Xiner Li, Masatoshi Uehara, Xingyu Su, Gabriele Scalia, Tommaso Biancalani, Aviv Regev, Sergey Levine, and Shuiwang Ji. Dynamic search for inference-time alignment in diffusion models. *arXiv preprint arXiv:2503.02039*, 2025.

Runze Liu, Junqi Gao, Jian Zhao, Kaiyan Zhang, Xiu Li, Biqing Qi, Wanli Ouyang, and Bowen Zhou. Can 1b llm surpass 405b llm? rethinking compute-optimal test-time scaling. *arXiv preprint arXiv:2502.06703*, 2025.

João F. C. Mota, Nikos Deligiannis, and Miguel R. D. Rodrigues. Compressed sensing with prior information: Strategies, geometry, and bounds. *IEEE Transactions on Information Theory*, 2017.

Dongbin Na, Sangwoo Ji, and Jong Kim. Unrestricted black-box adversarial attack using gan with limited queries. In *European Conference on Computer Vision*, 2022.

Long Ouyang, Jeffrey Wu, Xu Jiang, Diogo Almeida, Carroll Wainwright, Pamela Mishkin, Chong Zhang, Sandhini Agarwal, Katarina Slama, Alex Ray, John Schulman, Jacob Hilton, Fraser Kelton, Luke Miller, Maddie Simens, Amanda Askell, Peter Welinder, Paul F Christiano, Jan Leike, and Ryan Lowe. Training language models to follow instructions with human feedback. In *Advances in Neural Information Processing Systems*, 2022.

Samet Oymak, Christos Thrampoulidis, and Babak Hassibi. Simple bounds for noisy linear inverse problems with exact side information. *arXiv preprint arXiv:1312.0641*, 2013.

Alec Radford, Jong Wook Kim, Chris Hallacy, Aditya Ramesh, Gabriel Goh, Sandhini Agarwal, Girish Sastry, Amanda Askell, Pamela Mishkin, Jack Clark, et al. Learning transferable visual models from natural language supervision. In *International conference on machine learning*, 2021.

Rafael Rafailov, Archit Sharma, Eric Mitchell, Christopher D Manning, Stefano Ermon, and Chelsea Finn. Direct Preference Optimization: Your Language Model is Secretly a Reward Model. In *Advances in Neural Information Processing Systems*, 2023.

Robin Rombach, Andreas Blattmann, Dominik Lorenz, Patrick Esser, and Bjorn Ommer. High-Resolution Image Synthesis with Latent Diffusion Models . In *2022 IEEE/CVF Conference on Computer Vision and Pattern Recognition (CVPR)*, 2022.

Litu Rout, Negin Raoof, Giannis Daras, Constantine Caramanis, Alex Dimakis, and Sanjay Shakkottai. Solving linear inverse problems provably via posterior sampling with latent diffusion models. In *Advances in Neural Information Processing Systems*, 2023.

Litu Rout, Yujia Chen, Nataniel Ruiz, Abhishek Kumar, Constantine Caramanis, Sanjay Shakkottai, and Wen-Sheng Chu. RB-modulation: Training-free stylization using reference-based modulation. In *The Thirteenth International Conference on Learning Representations*, 2025.

Subham Sekhar Sahoo, Marianne Arriola, Yair Schiff, Aaron Gokaslan, Edgar Marroquin, Justin T Chiu, Alexander Rush, and Volodymyr Kuleshov. Simple and effective masked diffusion language models. In *Advances in Neural Information Processing Systems*, 2024.

Amrith Setlur, Chirag Nagpal, Adam Fisch, Xinyang Geng, Jacob Eisenstein, Rishabh Agarwal, Alekh Agarwal, Jonathan Berant, and Aviral Kumar. Rewarding progress: Scaling automated process verifiers for LLM reasoning. In *The Thirteenth International Conference on Learning Representations*, 2025.

David Silver, Aja Huang, Chris J Maddison, Arthur Guez, Laurent Sifre, George Van Den Driessche, Julian Schrittwieser, Sergey Ioffe, Alan Green, Xi Chen, and et al. Mastering the game of go with deep neural networks and tree search. *Nature*, 2016.

Raghav Singhal, Zachary Horvitz, Ryan Teehan, Mengye Ren, Zhou Yu, Kathleen McKeown, and Rajesh Ranganath. A general framework for inference-time scaling and steering of diffusion models. *arXiv preprint arXiv:2501.06848*, 2025.

Charlie Victor Snell, Jaehoon Lee, Kelvin Xu, and Aviral Kumar. Scaling LLM test-time compute optimally can be more effective than scaling parameters for reasoning. In *The Thirteenth International Conference on Learning Representations*, 2025.

Jascha Sohl-Dickstein, Eric Weiss, Niru Maheswaranathan, and Surya Ganguli. Deep unsupervised learning using nonequilibrium thermodynamics. In *Proceedings of the 32nd International Conference on Machine Learning*, 2015.

Bowen Song, Soo Min Kwon, Zecheng Zhang, Xinyu Hu, Qing Qu, and Liyue Shen. Solving inverse problems with latent diffusion models via hard data consistency. In *The Twelfth International Conference on Learning Representations*, 2024.

Jiaming Song, Chenlin Meng, and Stefano Ermon. Denoising Diffusion Implicit Models. In *International Conference on Learning Representations*, 2021a.

Jiaming Song, Arash Vahdat, Morteza Mardani, and Jan Kautz. Pseudoinverse-Guided Diffusion Models for Inverse Problems. In *International Conference on Learning Representations*, 2023a.

Jiaming Song, Qinsheng Zhang, Hongxu Yin, Morteza Mardani, Ming-Yu Liu, Jan Kautz, Yongxin Chen, and Arash Vahdat. Loss-Guided Diffusion Models for Plug-and-Play Controllable Generation. In *Proceedings of the 40th International Conference on Machine Learning*, 2023b.

Yang Song and Stefano Ermon. Generative modeling by estimating gradients of the data distribution. In *Advances in Neural Information Processing Systems*, 2019.

Yang Song and Stefano Ermon. Improved techniques for training score-based generative models. In *Advances in Neural Information Processing Systems*, 2020.

Yang Song, Jascha Sohl-Dickstein, Diederik P Kingma, Abhishek Kumar, Stefano Ermon, and Ben Poole. Score-based generative modeling through stochastic differential equations. In *International Conference on Learning Representations*, 2021b.

Evaggelia Tsiligianni and Nikos Deligiannis. Deep Coupled-Representation Learning for Sparse Linear Inverse Problems With Side Information. *IEEE Signal Processing Letters*, 2019.

Kevin E Wu, Kevin K Yang, Rianne van den Berg, Sarah Alamdari, James Y Zou, Alex X Lu, and Ava P Amini. Protein structure generation via folding diffusion. *Nature communications*, 2024.

Luhuan Wu, Brian L. Trippe, Christian A Naesseth, John Patrick Cunningham, and David Blei. Practical and asymptotically exact conditional sampling in diffusion models. In *Advances in Neural Information Processing Systems*, 2023.

Jiazheng Xu, Xiao Liu, Yuchen Wu, Yuxuan Tong, Qinkai Li, Ming Ding, Jie Tang, and Yuxiao Dong. ImageReward: Learning and Evaluating Human Preferences for Text-to-Image Generation. In *Advances in Neural Information Processing Systems*, 2023.

Haotian Ye, Haowei Lin, Jiaqi Han, Minkai Xu, Sheng Liu, Yitao Liang, Jianzhu Ma, James Zou, and Stefano Ermon. TFG: Unified Training-Free Guidance for Diffusion Models. In *Advances in Neural Information Processing Systems*, 2024.

Jiwen Yu, Yinhuai Wang, Chen Zhao, Bernard Ghanem, and Jian Zhang. FreeDoM: Training-Free Energy-Guided Conditional Diffusion Model. In *2023 IEEE/CVF International Conference on Computer Vision (ICCV)*, 2023.

Jure Zbontar, Florian Knoll, Anuroop Sriram, Tullie Murrell, Zhengnan Huang, Matthew J Muckley, Aaron Defazio, Ruben Stern, Patricia Johnson, Mary Bruno, et al. fastmri: An open dataset and benchmarks for accelerated mri. *arXiv preprint arXiv:1811.08839*, 2018.

Bingliang Zhang, Wenda Chu, Julius Berner, Chenlin Meng, Anima Anandkumar, and Yang Song. Improving diffusion inverse problem solving with decoupled noise annealing. *arXiv preprint arXiv:2407.01521*, 2024.

Kaipeng Zhang, Zhanpeng Zhang, Zhifeng Li, and Yu Qiao. Joint face detection and alignment using multitask cascaded convolutional networks. *IEEE Signal Processing Letters*, 2016.